We are IntechOpen, the world's leading publisher of Open Access books
Built by scientists, for scientists

6,900
Open access books available

185,000
International authors and editors

200M
Downloads

154
Countries delivered to

Our authors are among the

TOP 1%
most cited scientists

12.2%
Contributors from top 500 universities

CLARIVATE ANALYTICS
BOOK CITATION INDEX
INDEXED

WEB OF SCIENCE™

Selection of our books indexed in the Book Citation Index
in Web of Science™ Core Collection (BKCI)

Interested in publishing with us?
Contact book.department@intechopen.com

California Coastal-Cooling a Reverse Reaction from Global Warming General Circulation and Mesoscale Effects

Bereket Lebassi-Habtezion[1], Jorge González[2] and Robert Bornstein[3]
[1]Department of Environmental Earth System Science
Stanford University, Stanford, California
[2]Department of Mechanical Engineering, the City College of New York, New York
[3]Department of Meteorology, San José State University, San José, California
USA

1. Introduction

California complex-topography coastal-areas are influenced by mesoscale coastal flows, initiated by near-surface (herein referred to as "surface") temperature differences between land and ocean that produce onshore daytime sea breezes and off-shore nighttime land breezes (Pielke 1984). Related phenomena include return flows aloft, MBLs (all acronyms are defined in Appendix) and associated inversions, LLJs, upslope and down slope winds, and topographic channeling (Mahrer and Pielke 1977). These phenomena depend on time of year, latitude, SSTs, PBL-depth and -stability, and factors that alter land-surface energy balances (e.g., clouds, land use, albedo [α], and soil moisture). SoCAB sea breezes have been extensively documented, e.g., a shallow coastal MBL that deepens inland (Edinger 1959) and cool marine air that warms as it advances inland, until its frontal inversion weakens and finally erodes (Edinger 1963).

These SoCAB mesoscale phenomena have also been modeled, e.g., Ulrickson and Clifford (1990) found that summer daytime upslope flows ventilate the Basin by merging with and strengthening sea breeze flows. This flow converges at inland mountain tops, producing strong vertical motions, which create return offshore-directed flows. Polluted air is prevented from exiting the SoCAB (in the pass between the San Gabriel and San Bernardino Mountains) by opposing upper level easterly-flows associated with mesoscale highs north of that gap (Boucouvala et al. 2003).

Observational analyses have indicated that cooling of JJA maximum temperature (T_{max} values) in coastal California over the last several decades could be due to increased: irrigation (Bonfils and Lobell 2007), coastal upwelling (Bakun 1990), stratus cover (Nemani et al. 2001), and/or urban cool-islands (LaDochy 2007). Lebassi et al. (2009), however, showed that this cooling from 1970-2005 was due to a "reverse reaction" to GHG induced-warming of inland areas, which increases sea breeze activity that overwhelms the warming in low-elevation SFBA and SoCAB coastal areas (see Fig. 1 for SoCAB). Irrigation is not a factor in these coastal areas, but increased upwelling, cold air advection, and stratus changes probably contribute to this observed cooling. Their results for all 253 California COOP sites together showed increased

(0.15°C decade⁻¹) T_{ave}-values; asymmetric warming, as minimum temperature (T_{min}) values increased faster than T_{max}-values (0.27 vs. 0.04°C decade⁻¹); and thus decreased DTR values (-0.23°C decade⁻¹). While JJA nighttime SoCAB and SFBA minimum temperatures T_{min} showed expected GHG-induced warming, their T_{max}-values exhibited a complex spatial pattern, with cooling (-0.30°C decade⁻¹) in low-elevation coastal-areas open to marine air penetration and warming (0.32°C decade⁻¹) at inland areas, which suggests that the inland warming resulted in increased coastal sea-breeze activity. Lebassi et al. (2010) showed that per capita energy consumption for summer cooling in the two coastal-cooling areas decreased during the period, while it increased in inland warming areas.
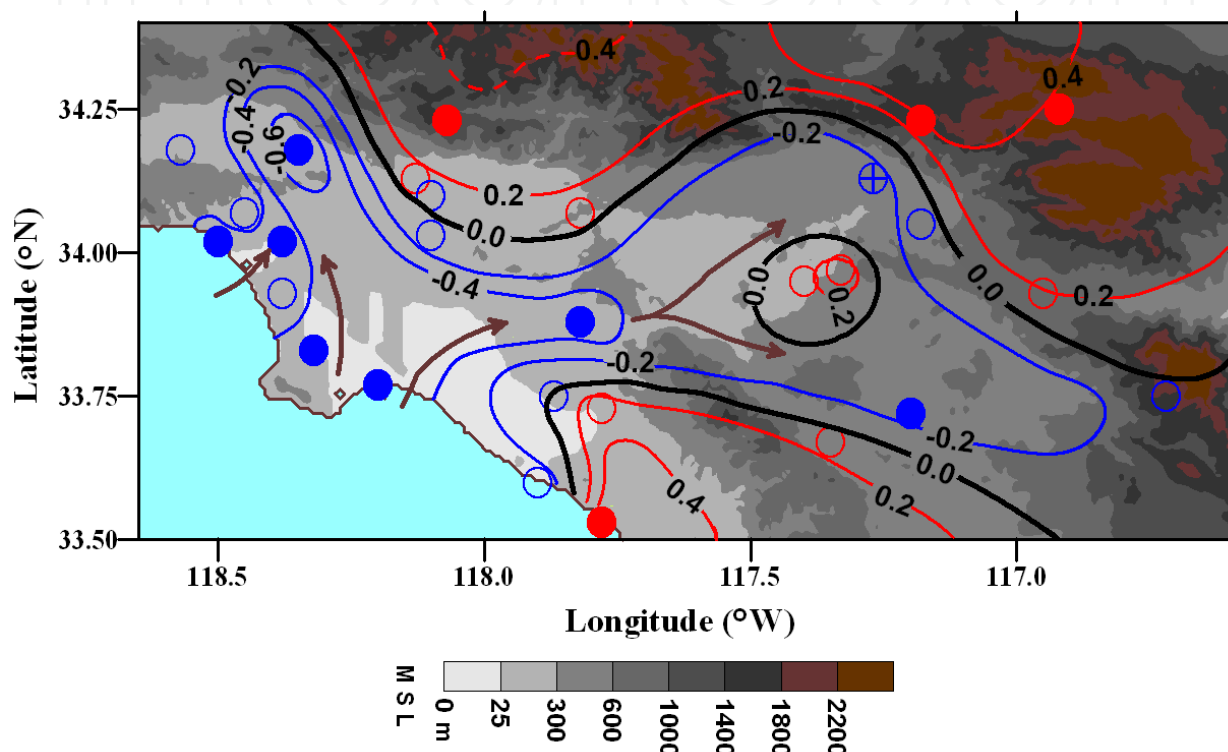

Fig. 1. Spatial distribution of observed SoCAB 2-m summer maximum-temperature trends (°C decade-1) for 1970-2005; arrows indicate predominant summer daytime surface-flow patterns; blue, red, and black colors indicate cooling, warming, and no-change isopleths and station locations; dashed isopleths are extrapolated; and statistical significance values of >99%, between 95 and 99%, between 90 and 95%, and < 90% are represented, respectively, by full-colored, half-colored, plus sign in circles, and open circles; from [Lebassi et al., 2009].

GCM simulations by Cayan et al. (2008) project a total 21st century warming of 2-5°C for California surface temperatures. Downscaled regional climate modeling by Kueppers et al. (2007) showed western-US irrigation lowering average temperature (T_{ave}) and T_{max} values at rates comparable to the increases from GHG warming. Similar modeling by Miller et al. (2003) showed California T_{ave} warming rates of 2.1-4.5°C, while ensemble downscaling by Maurer (2007) of 1950-99 JJA median temperatures showed warming rates that decreases from 0.13°C decade-1 in inland California to 0.08°C decade-1 at coastal areas north of the SoCAB. While this showed coastal influences, its coarse spatial resolution could not sufficiently resolve local topographic features that affect mesoscale circulations and thus local temperature trends. Local modeling by Lobell et al. (2006) showed California

temperature changes generally determined by GHG warming, but with large land-use changes locally dominant.

Mesoscale climate-change modeling by Snyder et al. (2003) and Duffy et al. (2006) showed increased GHG-warming strengthens onshore pressure and temperature gradients, as land areas warm faster than ocean areas due to thermal differences. Thus enhance alongshore winds strengthened upwelling, which further increased onshore temperature gradients. McGregor et al. (2007) observed this effect over coastal northwest Africa, while Bakun (1990) hypothesized a similar scenario to explain observed 30 year increases of California upwelling.

IPCC (2001) annual temperature trends for 1976-2001 do, in fact, show such cooling (up to 0.6°C decade[-1]) at all the west coast areas listed above, except Portugal. Recent local observational studies have also detected coastal cooling, e.g., Falvey et al. (2009) analyzed 1979-2006 NCDC and gridded observed (annual-average and maximum) temperature trends over coastal Chile, and found coastal-cooling. Coastal sediment-cores along Peru, analysed by Gutiérrez et al. (2011), also showed cooling SSTs for the latter part of the 20th century.

Oglesby et al. (2010) analyzed 4 km WRF modeled-differences (between 2000-2004 and 2050-2054), forced with CCSM output, for Meso-America; coastal cooling was predicted along the Pacific coasts of Mexico and Central America. This result indicates that the currently discovered SoCAB coastal cooling might likewise continue over the next 50 years, although a similar series of WRF simulations by Zhao et al. (2011) for all of California did not show coastal-cooling, perhaps because they forced their simulations with output from the older Parallel Climate Model (PCM) model.

While previous studies generally attributed observed JJA asymmetric warming in coastal California during the last three decades to increases in cloud cover, SSTs, upwelling, land use changes (i.e., urbanization, and/or irrigation); Lebassi et al. (2011) used the RAMS mesoscale meteorological model to quantify global warming effects on SoCAB summer sea breeze patterns and thus on T_{max} trends. Thus, this study analyzed large scale input data used by Lebassi et al. 2011) for a difference simulations between summertime past (1966-'70) and present (2001-'05) atmospheric fields of surface air temperature, sea surface temperature and pressure over California. The changes in the vertical profiles of temperatures, wind, marine boundary layer height and subsidence are quantified. This will increase the understanding of the changes in the vertical structure of the boundary layer and possibly impacts of these changes to coastal cooling.

2. Methodology

2.1 Model description

The overall goal of the current high-resolution RAMS mesoscale meteorological numerical-model simulations of current (i.e., 2001-05) and past (i.e., 1966-70) SoCAB summer sea breeze wind and temperature patterns is to analyzed the large scale forcings of the RAMS simulations and the vertical structures of coastal cooling.

An outer grid with a horizontal grid spacing of 16 km, and an inner grid of 4 km, are specified to capture larger scale (i.e., GC and synoptic) forcings and to further resolve more complex smaller mesoscale and urban phenomena, respectively. Simulations of 35 years of summer months are not feasible on such high resolution grids, because of the required large computational (i.e., one hour CPU time for one-day simulation-time with a 24 processor cluster) and storage resources. The current simulations are thus only for five consecutive summers during both a current (2001-05) and a past (1966-70) period. Resulting temperature and wind difference-fields are then quantified.

RAMS (Version 6.0), developed at CSU, solves the Reynolds-averaged quasi- Boussinesq, non-hydrostatic, primitive equations on a Polar stereographic map projection (Tripoli and Cotton 1986). It uses terrain-influenced sigma coordinates and an Arakawa-C staggered grid on which thermodynamic and moisture variables are defined at grid-volume centers, with velocity components on grid-face centers perpendicular to each component (Mesinger and Arakawa 1976).

Two fixed two-way interactive grids are centered over the SoCAB, with 30 vertical layers, stretched from a spacing of 0.03 to 1.2 km in the first 7.5 km (to increase near-surface uses time-split differencing (Pielke 1984), as well as a variable-field model initialization and update process, in which gridded 3-D fields of wind, potential temperature, and relative humidity values from a large-scale, i.e., NCEP in this application, model are assimilated at 6 h intervals via Newtonian relaxation (Davies 1983).

The cloud microphysics formulation of Walko et al. [1995] and Meyers et al. [1997] was used; as it includes complex parameterization of many ice species. A cumulus parameterization was not used, as both grid resolutions were at or below the 9-km resolution needing such formulations. Vertical diffusion coefficients were computed from the 2.5-level closure in Mellor and Yamada (1982), which employs a prognostic TKE equation. Short- and long-wave radiation were calculated following Mahrer and Pielke (1977), in which simulated water vapor and specified CO_2 concentrations affect radiative flux divergence optical-path calculations via their effects on atmospheric-emissivity.

The CO_2 concentration is assumed uniform in both domains at 330 ppm from the surface to 40 km, while down-welling long-wave flux at the model top is set to zero. The CO_2 value is comparable with the summer 329 ppm value observed by Keeling and Whorf (2004) at La Jolla, California in the early 1970s, while it underestimates the 2001 value of 369 ppm. Radiative effects from long-term global CO_2-increases, accounted for via the NCEP BCs, are ingested into RAMS every 6 hrs. Local inner-domain radiative effects from CO_2 trends are not accounted for, but should be small over the five-summer simulation period.

The 1966-1970 and 2001-2005 periods were selected for simulation, as they showed similar large-scale PDO climate-variability factors. Strong winter El Niños produce decreased coastal upwelling in southern California, while strong winter La Niñas produce the reverse (LadoChy et al. 2007). The more important multi-decaldal index influencing California summer climate, however, is the spring (MAM) PDO, evaluated from north Pacific SSTs. The JJA past- and present-periods were thus selected based on similarities between the trends of the anomalies of this index and those of coastal California JJA T_{ave}-values; i.e., both periods generally show small upward trends in both variables [*http://jisaao.washington. edu/ pdo/PDO.latest*].

2.2 Initialization, BCs, and statistical evaluation

RAMS was initialized with NCEP gridded data-sets, interpolated (offline) to its grid by its internal isentropic analysis package. The NCEP data contains the following 4-D fields on horizontal pressure surfaces at horizontal increments of 0.5 deg: horizontal velocity components, temperature, geopotential height, and relative humidity. These fields generate 3-D assimilation fields every 6 h during the execution (started at 2400 UTC; 1700 LT in summer) that nudge the coarse-grid lateral boundary-regions. Lateral BCs on the outer grid follow Klemp-Lilly (1978), a variant of Orlanski (1976), in which gravity-wave propagation speeds computed for each model-cell are averaged vertically, with the single average-value applied over the entire vertical column. In this scheme, horizontal diffusion coefficients are

computed as the product of horizontal deformation rate and length-scale squared (Smagorinsky 1963).

Initialization of RAMS also requires characterization of its surface BCs, via the following four input data sets, constructed "off line" and then interpolated to its 2-D surface grid-points:

- *Topography:* USGS topographic heights at a resolution of 30 arc-sec (about 1 km), obtained from the RAMS web site.
- *SSTs:* Monthly JJA ERSST, originally produced by statistical methods that allow for stable reconstructions from sparse data (Smith and Reynolds 2003) by use of ICOADS data. Values are down-loaded from NCDC at a resolution of 1-deg (about 111 km) for current-condition runs and at 2-deg for past–condition runs.
- *NDVI:* Monthly vegetation distributions, obtained from the RAMS web site on a 30 arc-sec grid.
- *LULC:* AVHRR data are used in the 1-km resolution Olson (1994) Global OGE 94-class LULC classification scheme, available from the USGS EROS Data Center (Lee 1992). OGE LULC data are input into the RAMS BATS scheme, which condenses its 94 classes into 21. OGE data are used in the outer-domain for the current-period simulations, but the inner-domain uses the 30 m resolution, 38-class, 2000 data from the NOAA C-CAP (http://www.csc.noaa.gov/digitalcoast/data/ccapregional/index.html). OGE LULC data are normally condensed to one urban and 20 rural classes in RAMS, but for the current simulations, two SoCAB urban LULC classes dominate: commercial and low-density residential; the one additional urban class was thus added to LEAF-3.

The LEAF-3 model (Walko et al. 2005) is used to calculate time-varying 2-D surface-temperature and -humidity BCs from linked prognostic surface-energy and -moisture balance equations for each of the following basic LULC type (i.e., group of similar classes): bare soil, plant-canopy covered soil, and urban; water surface temperature is assumed constant. Within any surface grid cell, 30-m patches are used to represent the heterogeneity of LULC classes. Once moisture and temperature values for each LULC category within each surface grid are calculated, the heat and moisture fluxes are area-averaged within each cell, used within SBL-parameterizations as (constant with height) fluxes, and finally used as the lower BCs for the sub-grid diffusion schemes in the finite-differenced prognostic PBL equations.

As the inner domain is mainly urbanized, the RAMS surface BCs were modified, to better account for urban processes, by the addition of a time- and spacing-varying Q_A for each urban sub-grid 30 m "patch." In US cities, Q_A is typically 60% from traffic sources; 40% from residential and industrial activities; and only a few percent from human metabolism (Sailor and Lu 2004). The current effort implements the time-varying daily profile, which shows morning and afternoon peaks associated with rush hour traffic.

RAMS look-up tables provide literature-values (as a function of LULC class) for the radiative, physical, vegetative, and thermal parameters associated with the surface-BC formulation. Values for several of key parameters for urban and rural LULC classes show increased values α and Vegetation height (H_v) values in urban areas.

As is the spatial distribution of vegetation fraction (F_v) is an important input-parameter, a technique was developed to determine it from high resolution Google™ earth-visible images as follows: (a) start with visible color Google map, (b) reduce map colors to 16, (c) count pixel values of each color in selected "typical" area for each urban class, (d) calculate fraction of green-color pixels to determine F_v, (e) reduce map colors to two (black and white), (f) count both the black and white pixels, (g) calculate fractions of white pixels to

determine rooftop fractions, and (h) calculate street fractions as black fraction minus vegetation fraction.

Only the F_v–value for each urban class can currently be input in the lookup table in RAMS. Further details can be found in Lebassi (2009).

An evaluation of RAMS-results at the 19-m level (i.e., lowest RAMS half-grid wind and temperature level) against 1-10 June 2002 (first 10-days of the "present" simulation) hourly observed 2-m temperatures and 10-m wind speeds from 12 SoCAB METAR weather stations was carried out by use of RAMS-values interpolated to those levels at the grid-point closest to each site. Daily-averaged surface temperatures from 15 COOP station had to be used to evaluate the past (1970) simulation results, as no hourly observations are available for that period. Both the RAMS 19-m level values and all observed values are hereafter referred to as "surface" values.

Spatial distributions of statistical significance-levels of RAMS-produced temperature and wind- differences (i.e., present minus past) in Domain-2 were also calculated. Mean-values and standard deviations of RAMS surface winds and temperatures were calculated for each Domain-2 grid-point at 1200, 1400, and 1600 LT over each five- or one-year (as appropriate) past and present simulation-period for use in Student-t significance tests of differences. The study focused on these hours, as they are the period of strongest sea-breeze impacts on the coastal temperatures.

3. Results

3.1 Model evaluation

A validation of present (1-10 June 2002) and past (JJA, 1970) model results against available surface observations was carried out. Figure 2 compares the time series of hourly average surface temperature and wind speed from the 12 SoCAB METAR stations for the period of the present simulations and daily surface temperatures from15 COOP station for the period of the past simulations with values from the RAMS grid point closest to each site. Due to the unavailability of observational data, only the daily maximum temperature is used to validate the past simulations.

Present RAMS temperatures (Fig. 2a) generally compare well with the observations [r^2=0.87, Fig. (2c)], as they capture diurnal cycles and day to day trends in peak-values. The 10 day average observed value was 19.1°C, while the modeled value was 20.3°C. RAMS captured the large-scale cooling trend over the first three days, the warming trend over the next four days, and the final three-day cooling trend. The largest discrepancies occurred on warm days, with overestimations of maxima by 2.5°C and minima by 2.0°C.

RAMS wind speeds (Fig. 2b) also compare well with observations, as they again generally capture diurnal cycles and daily peak values [r^2=0.8, Fig. (2c)]. The 10 days average observed value was 2.9 m s^{-1}, while the modeled value was 3.1 m s^{-1}. Minor discrepancies exist during the three hottest nights, which had observed near calm winds, when RAMS minima were about 1 m s^{-1}.

Past JJA daily maximum surface RAMS temperatures (Fig. 3) also generally compare well with the observations [r^2=0.7, Fig. (3a), blue], as they capture average JJA cycles and day to day trends in peak values. The JJA summer average T_{max} observed value was 26.5°C, while the modeled value was 27.3°C. RAMS captured the large-scale cooling trend over the first 13 days, followed by a warming trend over the next 13. The largest discrepancies again occurred on the warm days, with overestimations of maxima by 2.5°C and minima by 2.0°C.
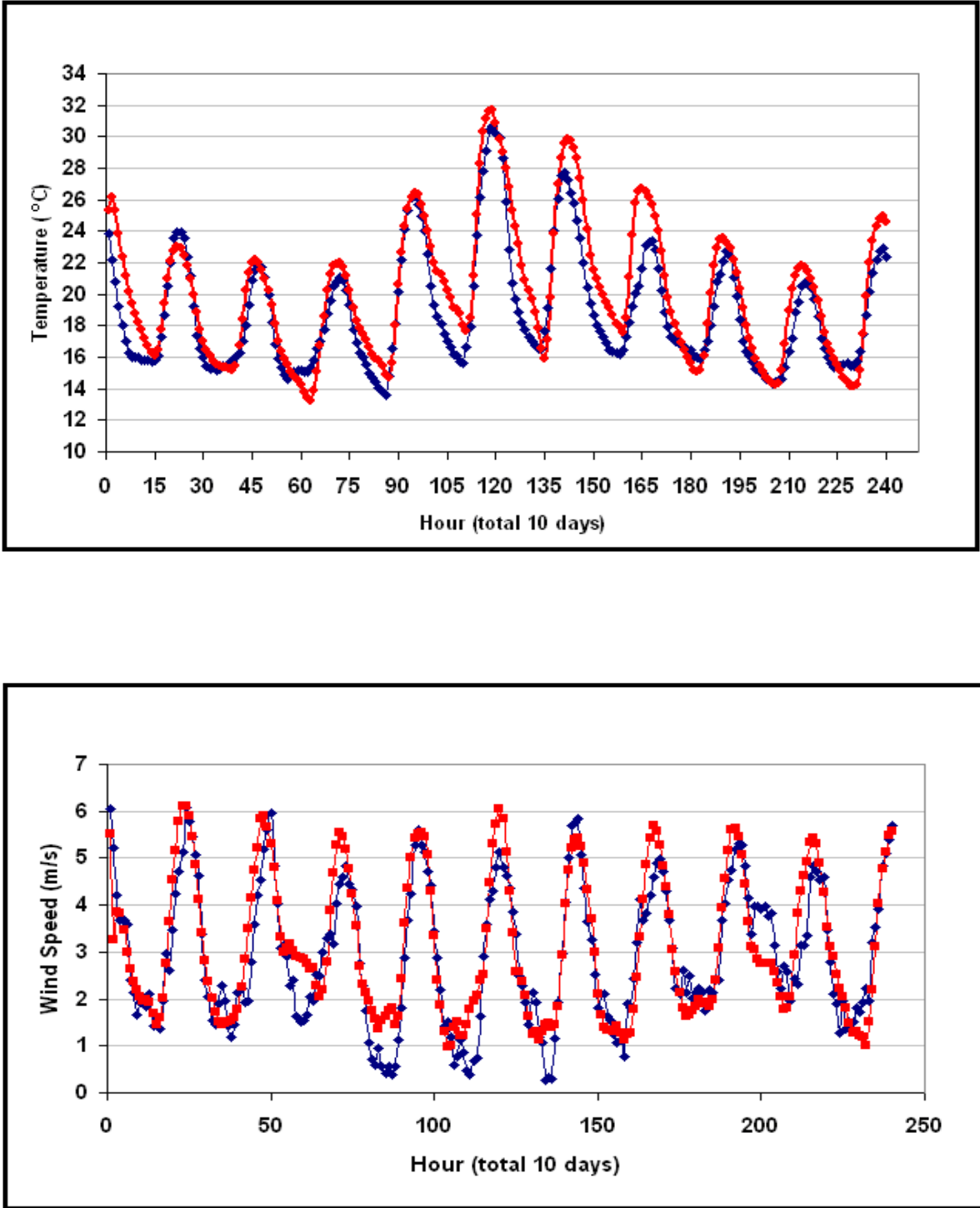
Fig. 2. a, b. (a) Modeled (red) vs. observed (blue) hourly 2-m temperatures (°C) averaged over 12 METAR stations for 1-10 June 2002; (b) same as Fig. 1a, but for wind speed (m s^{-1}).
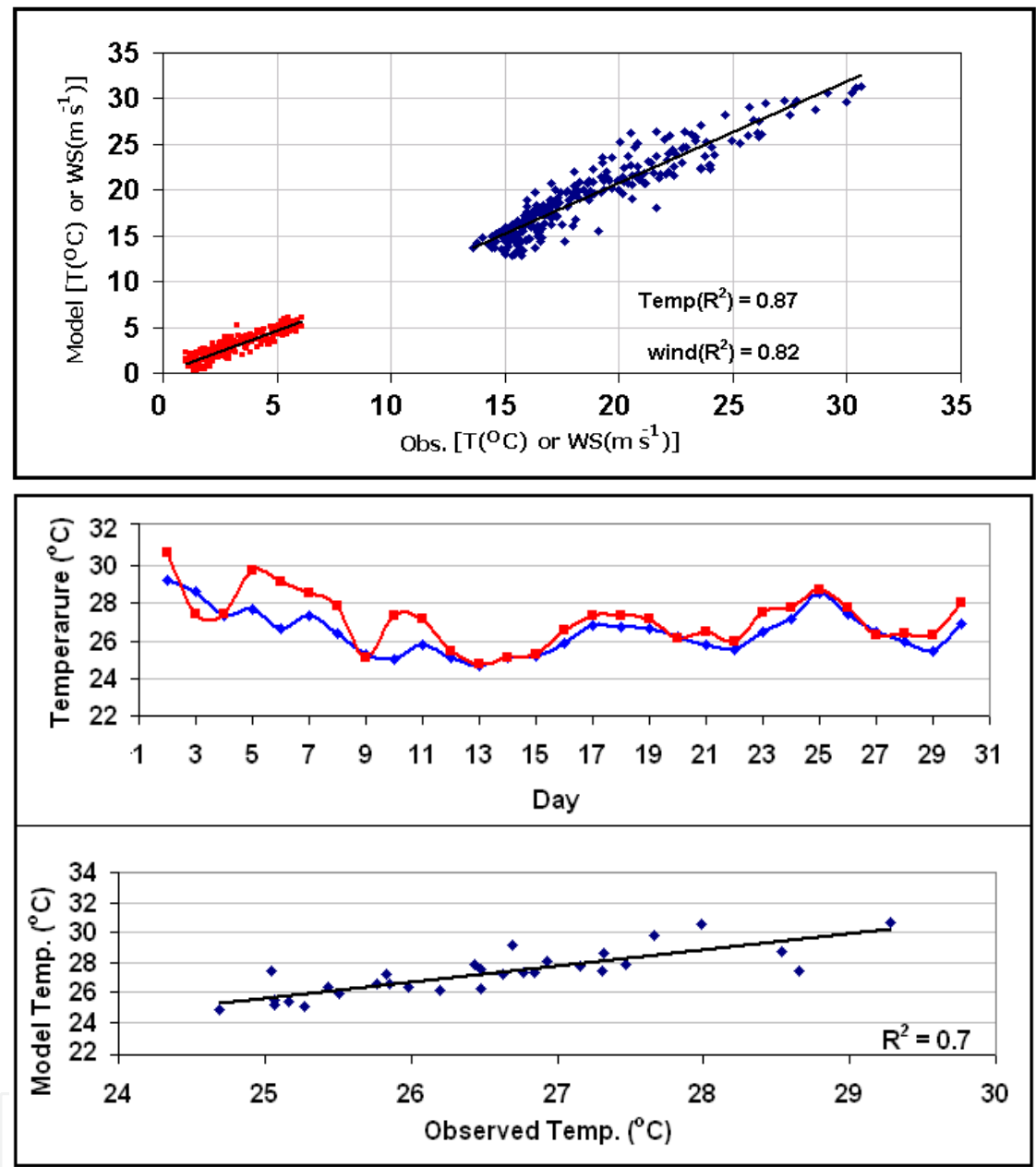
Fig. 3. a, b, c. (c) correlation of modeled vs. observed METAR temperatures (°C, blue) and wind speeds (red, m s⁻¹); (d) modeled (red) vs. observed (blue) daily 2-m summer temperatures (°C) averaged over 15 COOP stations; and (e) correlation plot of data in (d).

3.2 General circulation effects

GC forcing, the main external driver of the mesoscale RAMS model, enters through its initialization and BCs procedures. During summer, the semi-permanent Pacific High pressure system is located on its eastern edge, while a thermal low is over southeastern California. The resulting horizontal pressure gradient creates an onshore sea breeze flow over the SoCAB. This flow peaks in summer, when SSTs are coldest along the California coast within the southward flowing coastal California-current, as upwelling water reaches the surface as Ekman transport carries surface waters away from the coast.

NCEP 2.5 deg spatial-resolution sea level pressure p_s–values are interpolated from the input geopotential heights that initialize RAMS and provide its updated lateral BCs at 6 h intervals. The JJA-averaged 1000 hPa input NCEP p_s–values at 1700 LT for the five-year past-period of Run-2 shows the Pacific High centered west of California (Fig. 4a), with a central pressure center of 1024.3 hPa. The axis of the thermal low (central pressure of 1006 hPa) extends northward from Mexico to the California-Nevada border.
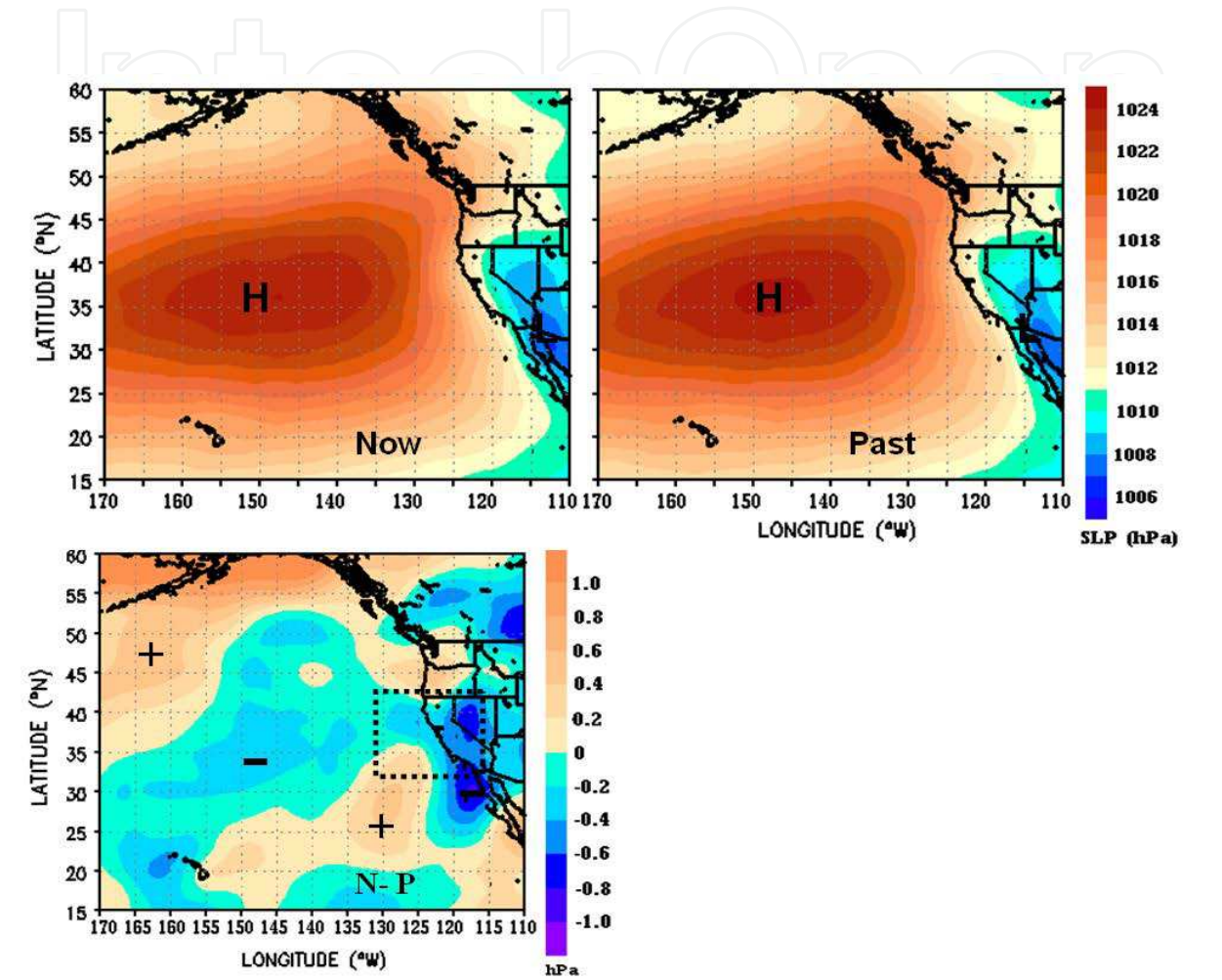
Fig. 4. Summer-averaged input NCEP 2.5-deg sea level pressures (hPa) at 17 LT, averaged over five-year periods of past and present simulations: (a) top right for past period, (b) top left for present period, and (c) lower for present minus past values (where pluses and minus denote increases and decreases, respectively).

The analogous input p_s field for the five-year present-period of Run-1 (Fig. 4b) shows the High basically unchanged in position and orientation, while the thermal low (as expected from the greater global warming over the continent) has extended northward (further into Nevada) and westward beyond the southern California-Mexico coast. Changes in p_s magnitude between the two simulations are best seen in Fig. 4c, in which the difference (herein defined as present minus past) pattern shows a broad region of decreased values of up to -0.4 hPa across the center of the High, north of a smaller area of increased values (up to 0.6 hPa). The two areas of decreased p_s in Nevada and along the coast (from the SoCAB to Mexico) are due to the expanding thermal low; over-water decreases peak at -1.0 hPa along

the Mexican coast. The thermal low, however, has expanded northward and southward, producing two areas of maximum pressure decreases (up to -1.0 hPa). It has also intensified and the pressure at its center has decrease by only -0.6 hPa, a smaller amount than both to the north (over Nevada) and south (over the SoCAB-Mexico coast). These input NCEP p_s changes produce an increased west to east large-scale pressure gradient over the area that will strengthen the onshore large-scale background flow, onto which RAMS-produced mesoscale thermally-driven flows will be superimposed.

The monthly-averaged ICOADS SSTs used as BCs in the RAMS Run-1 (present) and Run-2 (past) simulations have 2- and 1-deg spatial resolutions, respectively. Five-year average Domain-1 SSTs from the past-period Run-2 (Fig. 5a) show cold values (14°C) northwest of Domain-2 that increase southward (to 18°C).
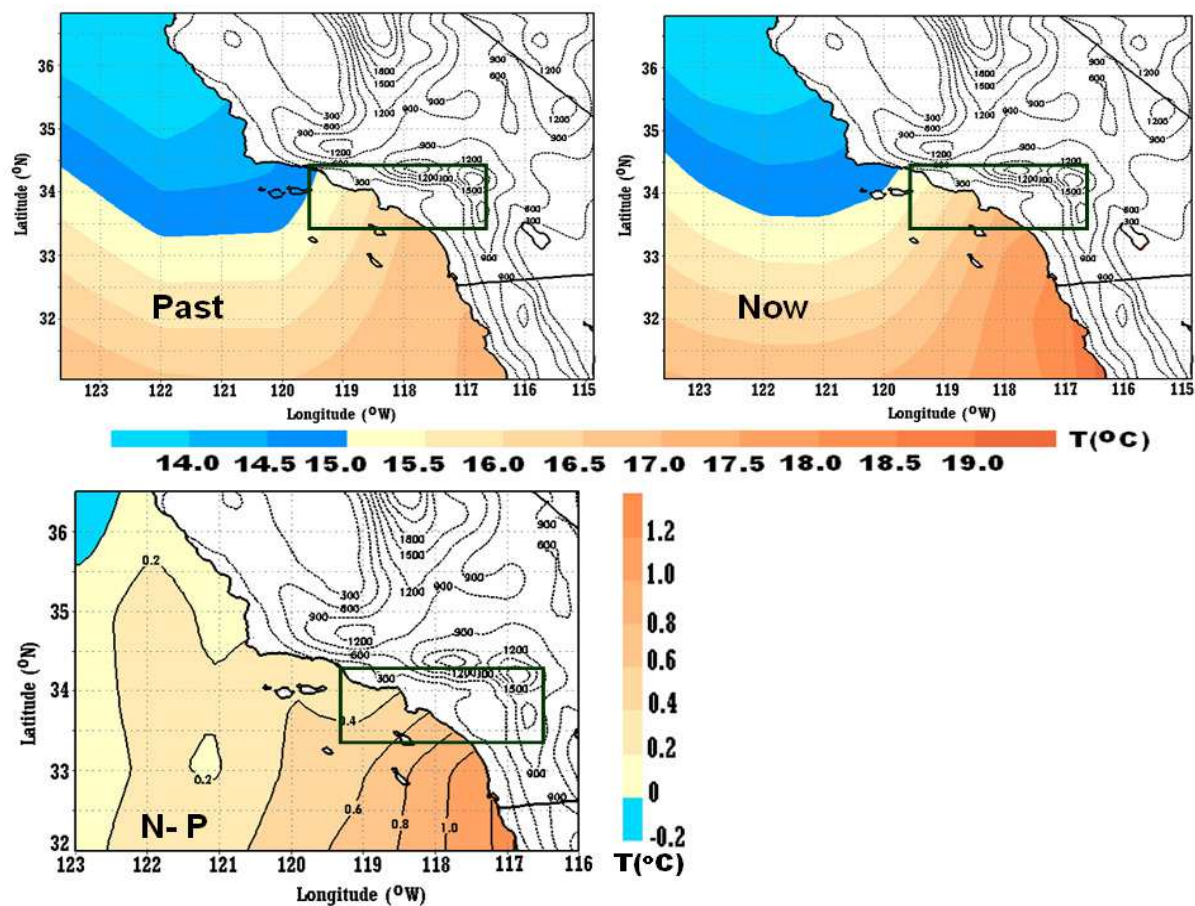

Fig. 5. Summer-averaged input ICOADS sea surface temperatures (°C) at 17 LT averaged over five-year periods of past and present simulations: (a) top left for past period (at 2 deg input resolution), (b) top right for present period (at 1 deg input resolution), and (c) lower for present minus past values; box represents Domain-2 area.

Present-period Run-1 results show cool-area values slightly reduced (Fig. 5b), with warm-area values increased. Differences (Fig. 5c) show the peak cooling at only -0.2°C, while the warming increased southward (up to 1.2°C). Global warming is expected, as others have observed increased SSTs over this period (e.g., Hansen 2006).

Averaged input JJA NCEP 1000-hPa temperatures 1700 LT for Run-2 (past) at a 2.5 deg spatial resolution (Fig. 6a) show cool ocean values (11 to 25°C), with warm land areas (25 to 41°C). The coldest area is west of SoCAB, while the warmest (41°C) is over Nevada. Run-1 (present) values show that the coldest ocean temperatures moved north-westward, while the hottest inland values moved southeast towards Arizona (Fig. 6b).
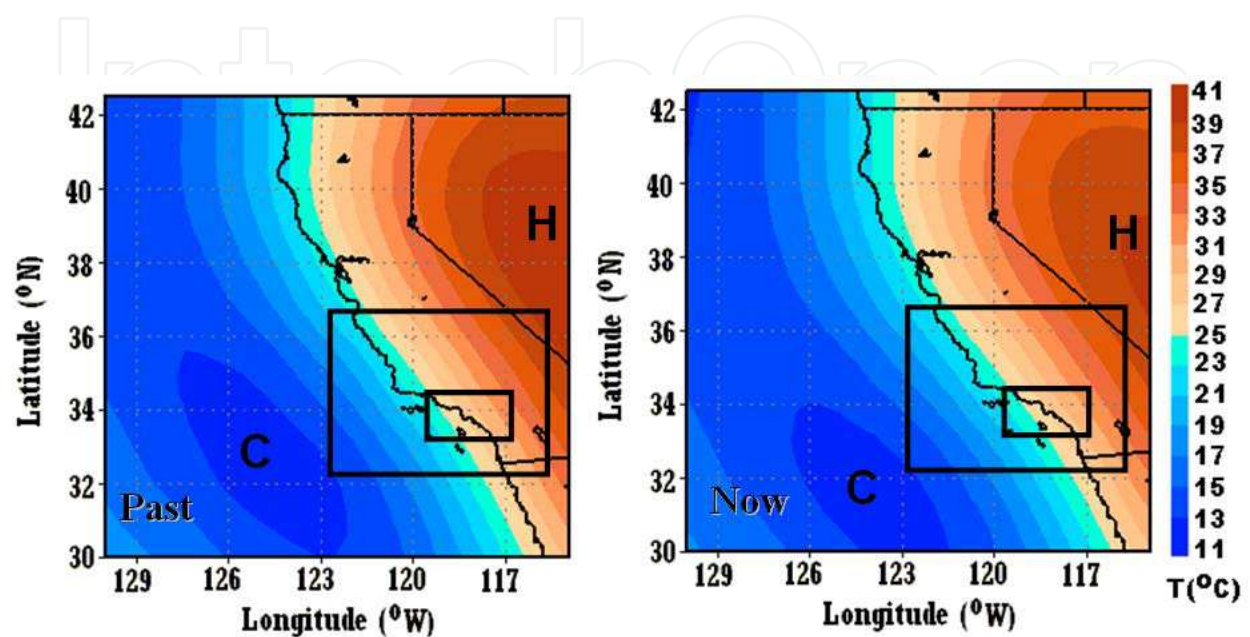

Fig. 6. Summer-averaged input NCEP 2.5 deg 1000-hPa temperature (°C) at 17 LT, averaged over five-year periods of past and present simulations: (a) right for past period and (b) left for present period; boxes indicate Domain 1 and Domain 2.

Differences (Fig. 7a) show cooling (up to -1.0°C) over the central ocean area, surrounded by a narrow band of warming ocean areas with values increasing (up to 0.6°C) southward along the coast from the SoCAB to Mexico. Over land, a narrow band of coastal areas (north SoCAB) showed slight cooling (up to -0.2°C), while inland areas warmed, with a maximum of 1.8°C over central Nevada. A vertical east-west cross section of these NCEP temperature changes at 34.0 N (Fig. 7b) shows the cooling over the coastal waters (up to -1.0°C) contained within the MBL (up to 925 hPa or 400 m); it also shows a local maximum global warming (1.2°C) at 900 hPa and an absolute peak (1.8°C) at 850 hPa. While global warming is expected, the cooling has not been found in previous observational or modeling studies (to the best of our knowledge), but is here-in hypothesized could be due to the southward movement of the Thermal Low in Fig. 4.

In summary, the large scale Pacific High is generally unchanged in position and orientation, but shows a diminished central pressure. JJA average 1700 LT NCEP temperatures at 1000 hPa showed cooling over the central California coast that extends up-wards to about 925 hPa. Finally, SSTs generally showed warming, which increased to the south. Vertical Profile of the NCEP data did not resolve the base of the marine boundary layer over the California coast. This large scale results are input for the model as ICs and BCs, and RAMS results in the next section will be analyzed to evaluate the vertical structure of GHG-induced coastal cooling.
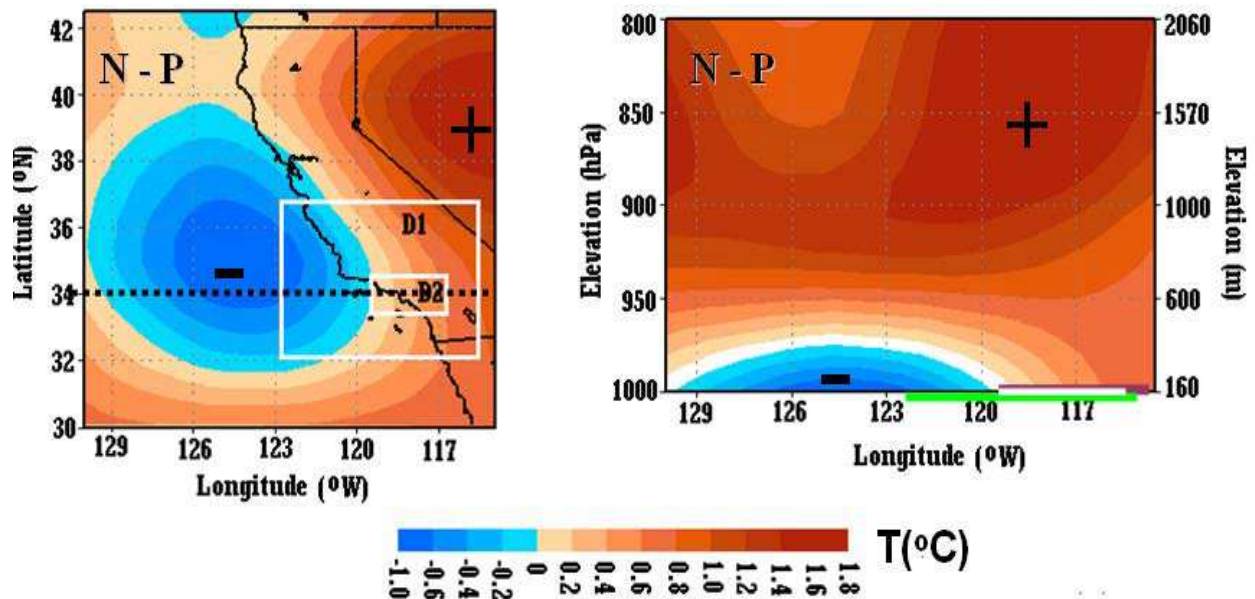
Fig. 7. Temperature changes (°C, past minus present) for values in plots in Fig. 6 in: (a) horizontal plane (right) and (b) vertical plane, shown by dashed line in (a).

3.3 MesoScale effects: Modeled vertical structure of coastal cooling

A cross-section at 33.83 N (through Domain-2) shows the vertical extents of MBL-changes and coastal cooling, i.e., the 1600 LT Run-2 (present) temperature results shows cold marine air (ex post facto defined, see below, as having temperatures ≤ 21°C) coming onshore and up against the coastal mountains (Fig. 8a).

The subsidence inversion top from the High is at about 750 m and at a temperature between 22 and 23°C. Its base is at the surface (i.e., at 19-m, the lowest RAMS temperature grid level), as opposed to several hundred meters. According to Thompson (2010, personal communication), this results as the RAMS TKE scheme does not generate sufficient mechanical turbulence over ocean areas. This occurred in the Coupled Ocean/ Atmosphere Mesoscale Prediction System (COAMPS) model (developed for over-ocean forecasting) until recent changes were made to its TKE formulation. Air temperatures above the inversion-top decreases to 20°C at 2 km.

The Run-1 (present) temperature cross-section (Fig. 8b) also shows a similar structure, but the inversion-base is now elevated to 60 m (i.e., second lowest temperature grid level), while the inversion-top has grown to 900 m, which could be due to the decreased subsidence discussed below. Near-surface temperatures at the higher inland-elevations have warmed by about 1°C, while those at 2 km have cooled by a similar amount, both of which are expected from global warming theory.

The corresponding difference plot (Fig. 8c) more accurately visualizes these relatively small temperature changes, i.e., a shallow layer (50 to 120 m) of over-ocean temperature increase (up to 0.4°C) exists, due to the increased SSTs discussed above and which causes formation of the shallow marine sub-inversion layer in Fig. 8b. Above this, a 450 m layer that has cooled (up to -1.0°C) resulted due to the large-scale cooling in the NCEP BCs (Fig. 6). Inland global warming peaks (at 1.4°C) at 2 km, while coastal cooling (up to -0.6°C) extends inland

to the top of the coastal hills. The cooling is due to the increased sea breeze activity, as unconnected at 19 m to the NCEP-introduced cooling. If the inversion-base was accurately reproduced, then the SST induced near-surface warming-layer in Fig. 8c would extent upwards by several hundred more meters, which would thus also show the disconnected-nature of these two cooling areas. The shallow over-ocean SST warming, large scale elevated-cooling, coastal cooling, and global warming where all significant at 99%, while the narrow transition layer was less significant (<90%) due to cancellation effects of coastal cooling and inland warming.
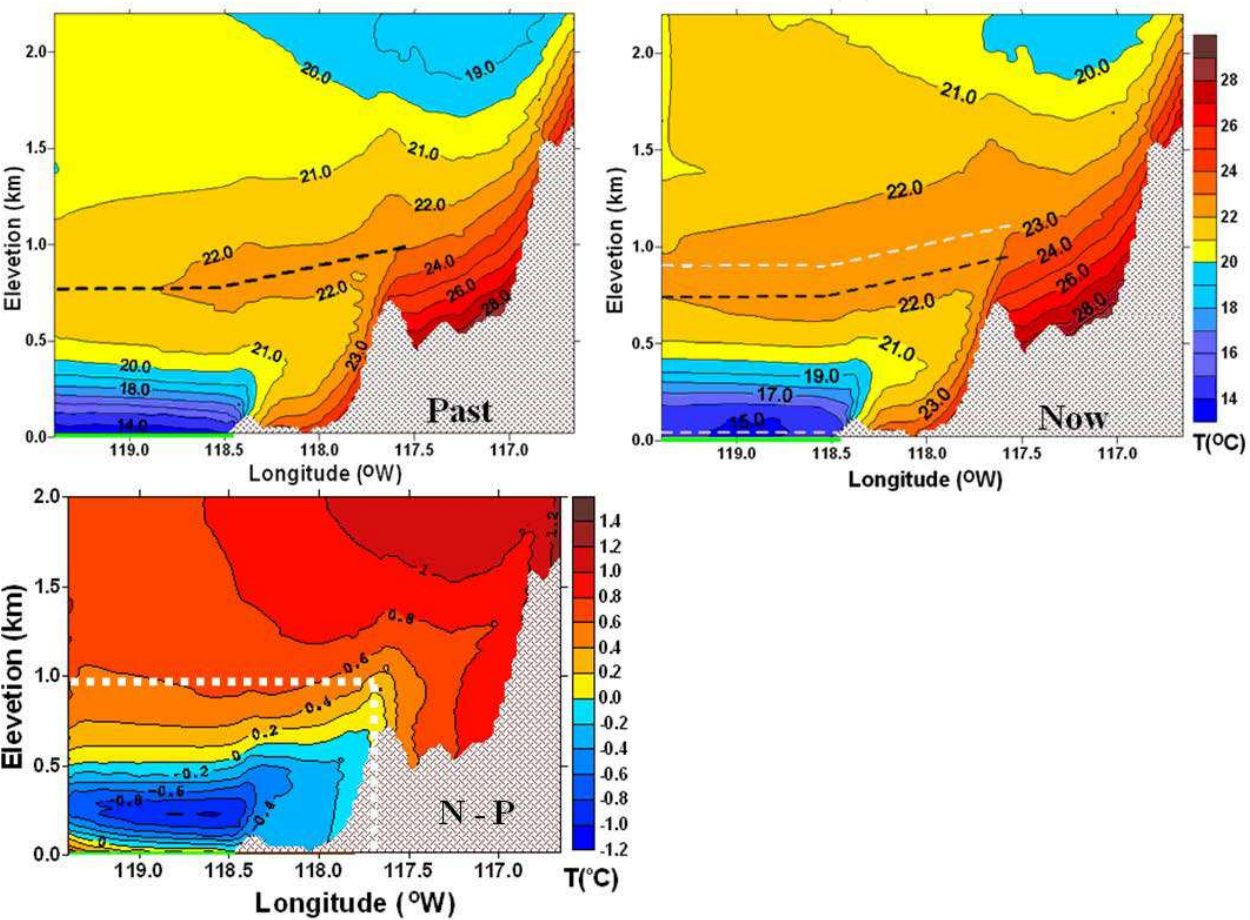

Fig. 8. Summer-averaged (over five-year periods of past and present simulations) Domain-2 temperature (°C) cross-section at 14 LT for Run-2 (past, top left) period, Run-1 (present, top right) period, and (c) present minus past (lower), where dashed lines represents inversion base and top and white dashed box represents area of D2 cross section at 33. 83 N (see Fig. 7 for location).

The vertical velocities in the vertical plane of Fig. 9 also showing the disconnected nature of the two cooling areas, i.e., the 1400 LT Run-2 (past) section (Fig. 9a) shows a peak subsidence from the High (up to -1.6 cm s^{-1}) over the ocean at 800 m, with peak upward motion areas over both the coastal plane and coastal topography (up to 3.6 cm s^{-1} above the

latter). Similar results are found for Run-1 (present) (Fig. 9b), but with a weaker subsidence (only up to -0.6 cm s^{-1}) over the ocean and decreased upward motion over coastal areas.

The "difference" vertical-velocity field (Fig. 9c) shows these changes more clearly, i.e., a maximum decreased of over-ocean subsidence of 0.6 cm s^{-1} at 500 m. The decreased upward motion over both land areas is also clearly shown, i.e., over the coastal basin and coastal mountains (both up to -0.6 cm s^{-1}), the former associated with the increased stability of the stronger sea-breeze flow. The decreased over-ocean subsidence is due to the extension of the Thermal Low in Fig. 4c.
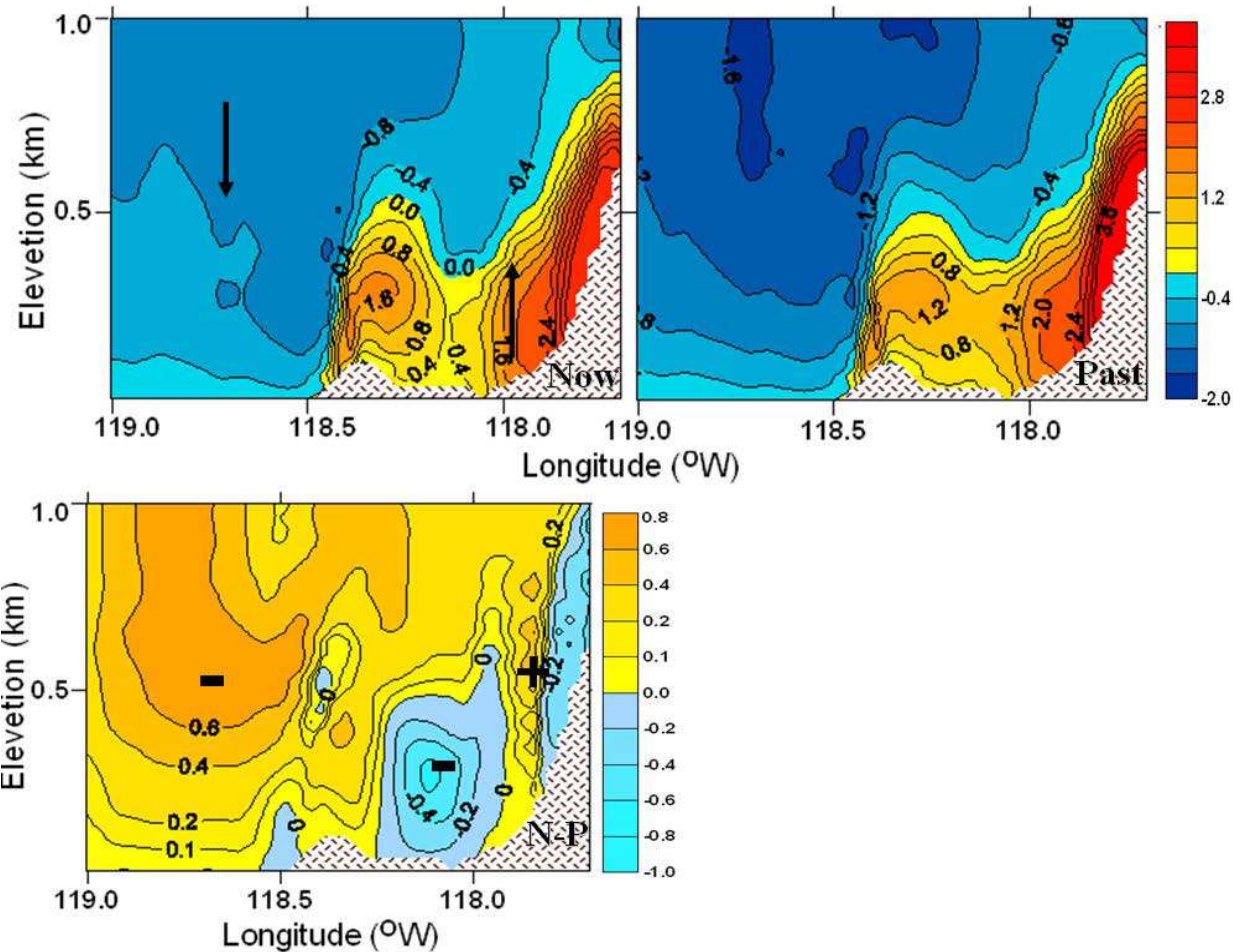

Fig. 9. Same as Fig. 8, but in sub-area of its white box and for vertical velocity values (cm s^{-1}) fields, where up/down arrows represent up/down motions and plusses/minuses represent increases/decreases, respectively.

4. Discussion and conclusion

The meso-met RAMS model was used to further investigate local (on 16 and 4 km grids) climate changes in the SoCAB, with simulations designed to quantify impacts from both global warming and urbanization. Results from a simulation with both present (2001-05)

summer climate-conditions and LCLU-patterns were compared to one with present-LCLU and past (1966-1970) climate.

Evaluation of model results against hourly surface temperature and wind speed observations during a current 10-day summer period showed that they captured diurnal cycles and day to day trends in peak and minimum values, with an exception on several warm days; average errors were only 1.2°C and 0.2 m s^{-1}, respectively. Evaluation of model results against past daily maximum temperatures averaged over 15 COOP stations also showed good agreement in trend and magnitude, with an average error of 0.7°C.

The shallow SST warming layer over the ocean, large scale elevated cooling, coastal cooling, and global warming were all significant at 99%. All transition-layers, in which two opposite effects cancel, showed less-significant (<90%) results.

NCEP input BCs to RAMS of summer 1000-hPa at 1700 LT showed that during the 35-years between the past and present simulation periods, the Pacific High was generally unchanged in position and orientation, but slightly diminished in central pressure (up to -0.4 hPa). The over-land Thermal Low expanded northward and southward, producing two areas of maximum pressure-decrease (up to -1.0 hPa) over Nevada and the SoCAB-Mexico coast. These input NCEP SLP-changes produced increased west to east large-scale pressure gradients that thus strengthened onshore large-scale background flows, onto which RAMS-produced mesoscale thermally-driven flows were superimposed.

ICOADS SSTs generally showed warming the 35-year period, which increased southward (up to 1.2°C) and which resulted from global warming. Concurrent input NCEP air temperatures generally showed a maximum global warming of 1.8°C at an elevation of 2-km over land areas. The warming extended downward to the surface over land areas, while a surface large-scale cooling over central California coastal waters (up to -1.0°C) extended upwards to about 925 hPa (or 400 m); effects from this imposed-cooling on RAMS results are discussed below.

Lebassi et al. 2009 in their observational study analyzed that average-JJA California land-surface min and max temperatures from 1970-2004 showed expected asymmetric-warming, with increases of 0.27 and 0.06°C decade^{-1}, respectively. The larger min-temperature increase was significant at the 93% level and was comparable with (and correlated to) the coastal daily-mean SST trend of 0.24°C decade^{-1} (significant at the 92% level). Different rates of max and min temperature increase is consistent with previously observed asymmetric global-warming from increased greenhouse-gasses. The spatial distribution of comparable observed SoCAB JJA max-temperatures, however, showed a more complex pattern, with both cooling at low-elevation coastal-areas open to marine air penetration and warming at inland and high-elevation coastal areas. The scarcity of observational sites in some parts of both regions meant for additional modeling study of the region. Lebassi et al. 2011 further modeled the SoCAB coastal cooling using the RAMS model and results captured many important aspects of the observed surface inland-warming and concurrent coastal-cooling that developed during the 35-years between the present and past summer-daytime simulation periods, i.e., sequentially: weaker global warming over the ocean than over inland areas, increased surface temperature gradients, strengthened sea breezes, and thus coastal cooling.

This study showed the vertical structure of coastal cooling in the finer RAMS domain. The model captured the vertical and horizontal extent of GHG-induced coastal cooling while

there is some limitations discussed below, which are introduced from the meso scale and forcing model, in this case NCEP. Fine-domain temperatures at 1400 LT showed an over-ocean Pacific High subsidence inversion-top that increased by 150 m (to a height of 900 m) over the 35-year period. Its base, however, was much below a reasonable MBL height (i.e., of several hundred meters). According to Thompson (2010, personal communication), these too low values resulted as the TKE scheme in RAMS does not generate sufficient mechanical turbulence over ocean surfaces, which also occurred in the COAMPS meso-met model (developed for over-ocean forecasting) until recent changes were made to its TKE formulation.

In addition, vertical profiles of NCEP temperatures showed that the model does not resolve the inversion base due the few number of grid point in the boundary layer. Even though further future research is needed to analyze the impacts of the large scale input on the mesoscale model, this could underestimate the base of the marine boundary layer which is several hundred meters in the coast of California. This study showed a too-shallow warming (over the 35-year period) layer of only 50 to 120 m thus developed over the ocean, as the increasing input-SSTs were unable to warm (and thus destroy) the lowest inversion layers and thus produce a realistically deep MBL. Above the lower warming layer, a 450 m layer cooled over the 35-years due to the large scale cooling within the input NCEP BCs. Over-land coastal cooling (to the same height) extended to the first coastal hill-tops due to the increased sea breeze activity. This cooling is unconnected to NCEP-introduced large-scale cooling, because the coarse-domain results showed separate areas for each effect.

The past vertical-velocity pattern showed peak subsidence (-1.6 cm s^{-1}) from the High over the ocean at 800 m, with peak upward motion areas over both the coastal plain (1.2 cm s^{-1} at 300 m) and first coastal topographic peak (>3.6 cm s^{-1} at 500 m). Similar present-simulation results were found, but with a smaller (reduction of up to -0.6 cm s^{-1}) subsidence over the ocean, in association with the decreased intensity of the High and the increased elevation of its inversion top, discussed above. The (present minus past) difference vertical-velocity field showed decreased upward motion over both the coastal basin and first coastal peaks, with the former associated with the increased stability from the more intense present-case cool stable marine-air sea breeze flow. These distinct vertical velocity difference-areas also demonstrate the disconnected nature of the two cooling areas.

In summary, the coarse domain RAMS results captured many important aspects of the observed surface and upper-level coastal cooling and inland warming that developed during the 35-years between the present and past simulation summer-daytime periods, i.e., sequential weaker global warming over the ocean than over inland areas, increased surface temperature gradients, strengthened sea breezes, and coastal cooling.

Various significance impacts may result from coastal cooling, e.g., summer daytime max ozone levels are decreased due to reduced rates of: fossil-fuel usage for cooling, natural hydrocarbon production, and photochemical photolysis. Agricultural production, water supply, and human thermal-stress and mortality are also effected by max summertime temperatures. Similar effects could exist in other coastal regions, while other regional reverse-reactions may be found in a variety of topo-climatic areas, possibilities that require further study. Future modelling efforts could enhance the current simulations by inclusion of finer scale horizontal grid resolutions and better large scale that resolved the marine boundary layer base.

5. Acknowledgments

6. References

Baklanov, A., B. Grisogono, R. Bornstein, L. Mahrt, S. Zilitinkevich, P. Taylor, S. Larsen, M. Rotach, and H. Fernando, 2010: On the nature, theory, and modelling of atmospheric planetary boundary layers. Accepted, *Bull. Amer. Met. Soc., 92,* 123-128.

Bakun, A., (1990), Global climate change and intensification of coastal ocean upwelling, *Science, 247*, 198–201, doi:10.1126/science.247.4939.198.

Bonfils, C., and D. Lobell, (2007), Empirical evidence for a recent slowdown in irrigation-induced cooling, *Proc. Natl. Acad. Sci., 104*, 13582-87, doi:10..1073/pnas.0700144104.

Bornstein, R. D., (1975), The two-dimensional URBMET urban boundary layer model, *J. Appl. Meteor., 14*, 1459-1477.

Bornstein, R. D., S. Klotz, U. Pechinger, R. Salvador, R. Street, L. J. Shieh, F. Ludwig, and R. Miller, (1986), Application of linked three-dimensional PBL and dispersion models to New York City, *Air Pollution Modeling and its Applications V*, Plenum Press, 543-564.

Boucouvala, D., R. Bornstein, J. Wilkinson, and D. Miller, (2003), MM5 simulations a SCOS97-NARSTO episode, *Atmos. Environ., 37*, S95–S117.

Cayan, D. R., E. P. Maurer, M. D. Dettinger, M. Tyree, and K. Hayhoe, (2008), Climate Change Scenarios for the California Region, *Climatic Change*, published online, doi:10.1007/s 10584-007-9377-6

Davies, H. C., (1983), Limitations of some common lateral boundary schemes used in regional NWP models, *Mon. Wea. Rev., 111*, 1002–1012.

Duffy, P. B., C. Bonfils, and D. Lobell (2007), Interpreting recent temperature trends in California, *Eos Trans. AGU, 88*, 409-410.

Edinger, J. G., (1959), Changes in the depth of the marine layer over the Los Angeles Basin, *J. of Meteor., 16*, 219-226.

Edinger, J. G., (1963), Modification of the marine layer over coastal southern California, *J. of App. Meteor.*, 16, 706-712.

Falvey, M., and R. D. Garreaud (2009), Regional cooling in a warming world: Recent temperature trends in the southeast Pacific and along the west coast of subtropical South America (1979–2006), *J. Geophys. Res., 114*, D04102, doi:10.1029/ 2008JD010519.

Gutiérrez, D., and et al. (2011), Coastal cooling and increased productivity in the main upwelling zone off Peru since the mid twentieth century, *J. Geophys. Res.*, *38*, L07603, doi:10.1029/2010GL046324, 2011.

Intergovernmental Panel on Climate Change (IPCC). (2001), IPCC Third Assessment Report - Climate Change 2001.

Keeling, C. D. and T. P. Whorf, (2004), Atmospheric CO_2 concentrations derived from flask air samples at sites in the SIO network. In Trends: A Compendium of Data on Global Change. Carbon Dioxide Information Analysis Center, Oak Ridge National Laboratory, U.S. Department of Energy, Oak Ridge, Tennessee, USA, 123 pp.

Klemp, J. B., and D.K. Lilly, (1978), Numerical simulation of hydrostatic mountain waves. *J. Atmos. Sci.*, *35*, 78-107.

Kueppers, L. M., M. A. Snyder, and L. C. Sloan, (2007), Irrigation cooling effect: Regional climate forcing by land-use change, *Geophys. Res. Lett.*, *34*, L03703, doi:10.1029/ 2006GL028679.

LaDochy, S., R. Medina, and W. Patzert, (2007), Recent California climate variability: spatial and temporal patterns in temperature trends, *Climate Research, CR 33*, 159– 169.

Lebassi, B., J. E. González, D. Fabris, E. Maurer, N. L. Miller, C. Milesi, P. Switzer, and R. Bornstein, (2009), Observed 1970-2005 cooling of summer daytime temperatures in coastal California, *J. Clim.*, *22*, 3558-3573, doi:10.1175/2008JCLI2111.1.

Lebassi, B. (2010), Observational and Modeling Study of Global Warming and Urbanization Impacts on Coastal California Climate, Ph.D. thesis, Dep. of Mech. Eng., Santa Clara Univ., Santa Clara, California.

Lebassi, B., J. E. Gonzalez, R. Bornstein, and, D. Fabris, (2010), Impacts of Climate Change in Degree Days and Energy Demand in Coastal California, *J. Sol. Energy Eng, 132*, 031005, doi:10.1115/1.4001564

Lebassi-Habtezion, B., J. E. Gonzalez, and R. Bornstein (2011), Modeled Large-Scale Warming Impacts on Summer California Coastal-Cooling Trends, *J. Geophys. Res., Accepted.*

Lee, R. L., and D. B. Olfe, (1974), Numerical calculations of temperature profiles over an urban heat island. *Bound.-Layer Meteor.*, *7*, 39-52.

Lobell, D. B., G. Bala, C. Bonfils, and P. B. Duffy, (2006), Potential bias of model project-ed greenhouse warming in irrigated regions, *Geophys. Res. Lett.*, *33*, L13709, doi:10.1029/ 2006GL026770.

Lobell, D., and C. Bonfils, (2008), The effect of irrigation on regional temperatures: A spatial and temporal analysis of trends in California, 1934–2002, *J. Clim., 21*, 2063-2071.

Mahrer, Y., and R. A. Pielke, (1977), The effect of topography on sea and land breezes in a two dimensional numerical model, *Mon. Wea. Rev., 105*, 115–1162.

Martilli, A., (2002), Numerical study of urban impact on the boundary layer structure: sen-sitivity to wind speed and urban morphology, and rural soil moisture, *J. Appl. Meteor., 41*, 1247-1267.

Masson, V., (2000), A physically-based scheme for the urban energy budget in atmospheric models. *Bound.-Layer Meteor.*, *94*, 357-397.

Maurer, E. P., (2007), Uncertainty in hydrologic impacts of climate change in the Sierra Nevada, California under two emissions scenarios, *Climatic Change, 82*, 309-25.

McGregor, H. V., M. Dima, H. W. Fischer, and S. Mulitzal, (2007), Rapid 20th-Century Increase in Coastal Upwelling off Northwest Africa, *Science, 315*, 637–639.

Mellor, G. L., and T. Yamada (1982), Development of a turbulence closure model for geophysical fluid problems, *Rev Geophys. Space Phys.*, *20*, 851-75.

Meyers, M. P., R. L. Walko, J. Y. Harrington, and W. R. Cotton (1997), New RAMS cloud microphysics parameterization. The two-moment scheme. *Atmos.* Res., 45, 3–39.

Mesinger, F., and A. Arakawa, (1976), *Numerical methods used in atmospheric models*, GARP Publication, No. 14, WMO/ICSU Joint Organizing committee, 64 pp.

Miller, N. L., K. Hayhoe, J. M. Jin, and M. Auffhammer, (2007), Climate change, extream heat, and electricity demand, *J. Appl. Meteor. and Climatology.*, *47, 6*, 1834-44.

Myrup, L., (1969), A numerical model of the urban heat island. *J. Appl. Meteor.*, 8, 908-18.

Nemani, R. R., M. A. White, D. R. Cayan, G. V. Jones, S. W. Running, and J. C. Cough-lan, (2001), Asymmetric warming over coastal California and its impact on the premium wine industry, *Climate Research*, *19*, 25–34.

Oglesby, R. J., C. M. Rowe, C. Hays, (2010), Using the WRF Regional Model to Produce High Resolution AR4 Simulations of Climate Change for Mesoamerica, A23F-07, Dec 14, 2010, San Francisco, CA.

Pielke, R. A., (1984), *Mesoscale Meteorological Modeling*. Academic Press, San Diego, California, 612 pp.

Sailor D. J., and L. Lu, (2004), A top-down methodology for developing diurnal and seasonal anthropogenic heating profiles for urban areas, *Atmos. Env.*, *38*, 2737–2748.

Smith, T. M., and R. W. Reynolds, (2003), Extended reconstruction of global sea surface temperature based on ICOADS data, *J. Climate, 16*, 1495–1510.

Snyder, M., L. Sloan, N. Diffenbaugh, and J. Bell, (2003), Future climate change and upwelling in the California current, *Geophys. Res. Lett.*, 30, 1823, doi:10.1029/ 2003GL017647.

Walko, R. L., W. R. Cotton, M. P. Meyers, and J. Y. Harrington (1995), New RAMS cloud microphysics parameterization. Part I: The single-moment scheme. *Atmos. Res., 38, 29–62.*

Taha, H., (1999), Modifying a mesoscale meteorological model to better incorporate urban heat storage: a bulk-parameterization approach, *J. Appl. Meteor.*, 38, 466-473.

Taha, H., (2007), Urban surface modification as a potential ozone air-quality improvement strategy in California: A mesoscale modeling study, *Bound. –Layer Meteor.*, *127*, 219-239, doi:10.1007/s10546-007-9259-5.

Tripoli, G. J., and W. R. Cotton, (1982), The Colorado State University three-dimensional cloud/mesoscale model – 1982. Part I: General theoretical framework and sensitivity experiments, J. *de Rech. Atmos., 16*, 185-220.

Ulrickson, B. L., and C. F. Mass (1990), Numerical investigation of mesoscale circulations in the Los Angeles Basin, Part I: verification study. *Mon. Wea Rev.*, *118*, 2238-61.

Walko, R. L., and C. J. Tremback, (2001), RAMS technical description, http://www.atmet. com/html/docs/rams/rams_techman.pdf.

Planet Earth 2011 - Global Warming Challenges and Opportunities for Policy and Practice

Edited by Prof. Elias Carayannis

The failure of the UN climate change summit in Copenhagen in December 2009 to effectively reach a global agreement on emission reduction targets, led many within the developing world to view this as a reversal of the Kyoto Protocol and an attempt by the developed nations to shirk out of their responsibility for climate change. The issue of global warming has been at the top of the political agenda for a number of years and has become even more pressing with the rapid industrialization taking place in China and India. This book looks at the effects of climate change throughout different regions of the world and discusses to what extent cleantech and environmental initiatives such as the destruction of fluorinated greenhouse gases, biofuels, and the role of plant breeding and biotechnology. The book concludes with an insight into the socio-religious impact that global warming has, citing Christianity and Islam.

How to reference

In order to correctly reference this scholarly work, feel free to copy and paste the following:

Bereket Lebassi-Habtezion, Jorge González and Robert Bornstein (2011). California Coastal - Cooling a Reverse Reaction from Global Warming General Circulation and Mesoscale Effects, Planet Earth 2011 - Global Warming Challenges and Opportunities for Policy and Practice, Prof. Elias Carayannis (Ed.), ISBN: 978-953-307-733-8, InTech, Available from: http://www.intechopen.com/books/planet-earth-2011-global-warming-challenges-and-opportunities-for-policy-and-practice/california-coastal-cooling-a-reverse-reaction-from-global-warming-general-circulation-and-mesoscale-

INTECH

open science | open minds